AGU PUBLICATIONS

JGR

Journal of Geophysical Research: Atmospheres

RESEARCH ARTICLE
10.1002/2016JD024824

Key Points:
- Bathymetry plays a role in Florida climate
- Florida's rainfall is dependent on Florida Current
- Rainy season varies by length of the season

Correspondence to:
V. Misra,
vmisra@fsu.edu

Citation:
Misra, V., and A. Mishra (2016), The oceanic influence on the rainy season of Peninsular Florida, *J. Geophys. Res. Atmos.*, *121*, 7691–7709, doi:10.1002/2016JD024824.

Received 19 JAN 2016
Accepted 21 JUN 2016
Accepted article online 23 JUN 2016
Published online 8 JUL 2016

The oceanic influence on the rainy season of Peninsular Florida

Vasubandhu Misra[1,2,3] and Akhilesh Mishra[1,2]

[1]Center for Ocean-Atmospheric Prediction Studies, Florida State University, Tallahassee, Florida, USA, [2]Department of Earth, Ocean and Atmospheric Science, Florida State University, Tallahassee, Florida, USA, [3]Florida Climate Institute, Florida State University, Tallahassee, Florida, USA

Abstract In this study we show that the robust surface ocean currents around Peninsular Florida, namely, the Loop and the Florida Currents, affect the terrestrial wet season of Peninsular Florida. We show this through two novel regional coupled ocean-atmosphere models with different bathymetries that dislocate and modulate the strength of these currents and thereby affect the overlying sea surface temperature (SST) and upper ocean heat content. This study show that a weaker current system produces colder coastal SSTs along the Atlantic coast of Florida that reduces the length of the wet season and the total seasonal accumulation of precipitation over Peninsular Florida relative to the regional climate model simulation, in which these currents are stronger. The moisture budget reveals that as a result of these forced changes to the temperature of the upper coastal Atlantic Ocean, overlying surface evaporation and atmospheric convection is modulated. This consequently changes the moisture flux convergence leading to the modulation of the terrestrial wet season rainfall over Peninsular Florida that manifests in changes in the length and distribution of daily rain rate of the wet season. The results of this study have implications on interpreting future changes to hydroclimate of Peninsular Florida owing to climate change and low-frequency changes to the Atlantic meridional overturning circulation that comprises the Loop and the Florida Currents as part of its upper branch.

1. Introduction

It is a well-known fact that Peninsular Florida (PF) is in the near vicinity of strong surface boundary currents (the Loop Current and the Florida Current system) and relatively warm coastal sea surface temperatures (SSTs) [*Gordon*, 1967; *Mooers*, 1998]. These current systems comprise part of the upper limb of the Atlantic Meridional Overturning Circulation (AMOC). The Yucatan Channel, upstream of the Florida Straits, is between the Mexican Yucatan Peninsula and Cuba. The oceanic flow through this channel forms the Loop Current that intrudes into the Gulf of Mexico before outflowing through the Florida Straits as the Florida Current. Recently, *Rousset and Beal* [2010], using ship-based observations, indicated that the volume transport through the Yucatan Channel and the Florida Straits are comparable to each other contrary to many of the previous studies [*Schlitz*, 1973; *Candela et al*., 2003]. *Rousset and Beal* [2010] also showed that the two currents exhibit similar seasonal variability with maximum in summer preceded and followed by a minimum in spring and fall seasons.

The role of the warm Atlantic coastal SSTs in the intensification of tropical cyclones is well known [*Bright et al*., 2002]. *Bright et al*. [2002] indicate that a large fraction of category 2 and weaker Atlantic cyclones intensify when they track along the Gulf Stream. PF is one of the unique regions in the continental United States (CONUS) that exhibits a distinct seasonal cycle of rainfall and a rather long wet season [*Misra and DiNapoli*, 2013]. The robustness of this seasonal cycle allows for defining the onset and demise dates of the wet season based on rainfall that is otherwise not possible in the higher latitudes of the CONUS. Using observations, *Misra and DiNapoli* [2013] noted that the wet season in parts of southeastern PF could stretch for as long as 6 months, spanning the summer (June-July-August (JJA)) and the fall (September-October-November) seasons.

There is considerable interest in understanding the potential impacts of climate change in Florida for several reasons including the future impact of Atlantic tropical cyclones, sea level rise, and storm surge in a future warm climate [*Misra et al*., 2011a; *Misra*, 2013]. Equally important, however, is the information on how seasonal rainfall patterns and intensity would change in a changing climate that could potentially have significant implications on the ecology and habitat of the biota [*Cameron-Devitt et al*., 2011]. Another reason for the quest to understand these impacts in Florida is also because of the rising coastal population of the state

Table 1. Outline of the Physics in RSM

Atmospheric Model (RSM) Physics	Reference
Gravity wave drag	*Alpert et al.* [1988]
Boundary layer	*Hong and Pan* [1996]
Deep convection	*Moorthi and Suarez* [1992]
Longwave radiation	*Chou and Suarez* [1994]
Shortwave radiation	*Chou and Lee* [1996]
Shallow convection	*Tiedtke* [1983]
Land surface process	*Ek et al.* [2003]

and changing (aging) demography that raises the vulnerability of the population to climate variability and change [*Cutter and Emrich*, 2006; *Pielke et al.*, 2008].

PF receives one of the highest rates of land falling tropical cyclones in the CONUS [*Larson et al.*, 2005; *Knight and Davis*, 2009; *Misra and Bastola*, 2015]. Therefore, it is obvious that a relatively large fraction of the wet season rainfall in Florida is a result of the rain from the land falling tropical cyclones, especially in South Florida, when examined over a number of years [*Knight and Davis*, 2009; *Maxwell et al.*, 2012, 2013; *Ortegren and Maxwell*, 2014]. Therefore, it is potentially difficult to estimate the wet season rainfall over Florida from climate models on seasonal to longer time scales because climate models are not reliable in simulating the tracks and intensities of the Atlantic tropical cyclones beyond the numerical weather prediction time scales [*Rappaport et al.*, 2010; *DeMaria et al.*, 2014]. However, a significant fraction of the wet season rainfall over PF also arises from diurnal variations that set up the sea breeze circulations along the coast [*Pielke*, 1974; *Burpee and Lahiffi*, 1984; *Blanchard and López*, 1985; *Misra et al.*, 2011b; *Bastola and Misra*, 2013; *Selman et al.*, 2013]. In the early part of the wet season, warm (cold) El Niño–Southern Oscillation (ENSO) events are associated with early (late) onset of the rainy season over south Florida resulting in longer (shorter) wet season [*Misra and DiNapoli*, 2013]. In the middle and later part of the wet season, tropical Atlantic variations dominate the variability of rainfall over Florida, while ENSO has less influence [*Misra and DiNapoli*, 2013].

A number of studies have highlighted the covariation of SST and convective rainfall. For example, *McBride and Fraedrich* [1995] suggest a SST threshold of 25.5°C that allows for a transition of the convective instability to grow from slow to fast mode. Similarly, *Erfani and Mitchell* [2014] showed that increase in SST in Gulf of California causes the disappearance of the inversion atop the marine boundary layer, allowing for the enhancement of moisture in the free troposphere as a precursor to the rainfall intensification over Arizona and northwestern Mexico. Likewise, in the observational study of *Black et al.* [2003] it is shown that a strong relationship exists between tropical Indian Ocean SST and east African short rains. This study is adding to this growing body of literature on impact of SST on near-local rainfall.

The purpose of this paper is to highlight the impact of the modulation of the Loop and the Florida Current system on the terrestrial wet season rainfall over PF. These currents essentially bring warm water from the tropical Atlantic (the Caribbean Sea) to the subtropical region (Gulf of Mexico and parts of northwestern Atlantic Ocean [*Mooers*, 1998]). We illustrate this impact by intercomparing two independent coupled ocean-atmosphere Regional Climate Model (RCM) multidecadal simulations, which display different ocean circulation in the Intra-Americas Seas (IAS; comprising the Gulf of Mexico and the Caribbean Sea) and northwest subtropical-tropical Atlantic Ocean to understand its impact on the wet season rainfall over Florida.

In the following section we will discuss the data sets and the methodology followed by discussion of results in section 3. Section 4 will present a summary of the findings with some concluding remarks.

2. Methodology and Data Sets

2.1. Regional Climate Model

2.1.1. Model Description

The regional coupled ocean-atmosphere model we have adopted for this study is the Regional Spectral Model-Regional Ocean Modeling System (RSM-ROMS [*Li and Misra*, 2014]). The RSM-ROMS has been widely used for regional coupled integrations over California and northeast Pacific Ocean [*Li et al.*, 2012, 2013, 2014] and over the Intra-Americas Seas [*Li and Misra*, 2014]. The RSM, which is the atmospheric component of the coupled model, is a primitive equation model on a stereographic projection that uses sine-cosine series as the horizontal basis function with a terrain-following vertical coordinate system of 28 sigma levels [*Juang and Kanamitsu*, 1994]. It has, however, gone through several upgrades in its parameterized atmospheric physics and dynamical core over the years. The readers are referred to *Kanamitsu et al.* [2010] for further details on the RSM. A brief outline of the physics of the RSM used in this study is provided in Table 1. The choice of these schemes stems

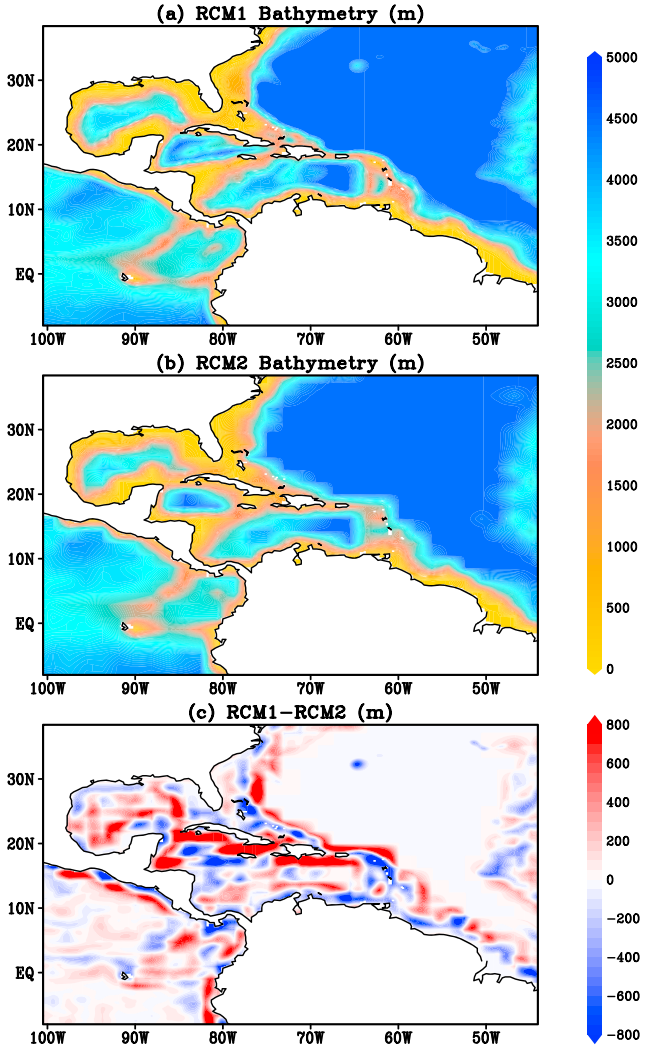

Figure 1. The bathymetry (in meters) used in (a) RCM1 and (b) RCM2 integrations and (c) their difference Figure 1a minus Figure 1b.

from previous successful simulations over the region [*DiNapoli and Misra*, 2012; *Selman et al.*, 2013; *Selman and Misra*, 2015].

The ocean component of the coupled model, ROMS version 3.0, is a free-surface, terrain-following, primitive equation ocean model [*Haidvogel et al.*, 2000; *Shchepetkin and McWilliams*, 2005]. The equations are solved using the split-explicit time-stepping scheme. The primitive equations are discretized in the vertical by using stretched, terrain-following coordinates. There are 30 sigma levels in ROMS. The ROMS contain several subgrid parameterizations, which include local closure schemes based on the level 2.5 turbulent kinetic energy equations [*Mellor and Yamada*, 1982] and generic length-scale parameterization following *Umlauf and Burchard* [2003]. The nonlocal closure scheme is based on the K profile, boundary layer formulation developed by *Large et al.* [1994]. The K profile scheme has been expanded to include both surface and bottom oceanic boundary layers.

The RSM and ROMS are coupled to each other with a coupling interval of 24 h. The atmospheric fluxes and SST are directly exchanged between RSM and ROMS without the use of any flux coupler. The RSM and ROMS share identical domain and horizontal resolution, which avoids periodic interpolation of the variables exchanged between the two components of the coupled model.

2.1.2. Experiment Design

In this study two separate integrations of the RSM-ROMS at 15 km grid resolution are conducted with identical domain but with separate bathymetries (Figure 1). One of them will be called RCM1 and the other RCM2. The RCM1 integration has been extensively verified with observations in *Li and Misra* [2014], and therefore, we will focus on the differences of this simulation from RCM2. Both these integrations are conducted for a 32 year period from 1979 to 2010. In both these integrations we use the 6-hourly atmospheric fields of the National Centers for Environmental Prediction-Department of Energy atmospheric reanalyis (NCEP-R2 [*Kanamitsu et al.*, 2002]) as the lateral boundary condition for the RSM, which is available at 2.5° grid spacing on 28 terrain-following sigma levels. We are able to force the RSM at such coarse resolution without multiple nesting because of a unique spectral nudging factor called the scale selective bias correction (SSBC [*Kanamaru and Kanamitsu*, 2007]). SSBC nudges the largest spatial scales in the regional domain of the RSM to the corresponding values of the lateral boundary forcing, thereby reducing the drift in the regional climate simulation, which otherwise could be significant [*Kanamaru and Kanamitsu*, 2007]. Similarly, we use the monthly mean Simple Ocean Data Assimilation version 2.2.4 (SODA) [*Carton and Giese*, 2008] as the lateral boundary forcing for ROMS. SODA is available at 0.5° grid spacing on 40 z levels. The initial conditions for RSM-ROMS are interpolated from the corresponding global atmospheric (NCEP-R2) and oceanic reanalysis (SODA) for 1 January 1979. These initial conditions are identical for both RCM1 and

RCM2. We, however, neglect the first 5 years of the model integration for the analysis of the results to account for spin-up issues. Therefore, we use the 1984–2010 (27 years) time period for the analysis of the results discussed in this paper.

In both RCM1 and RCM2 the source of the bathymetry is from Earth's surface topography and bathymetry on 5 min latitude-longitude grid (http://www.ngdc.noaa.gov/mgg/global/etopo5.HTML; Figures 1a and 1b). However, in RCM1 we smooth this bathymetry by running a five-point smoother once before interpolating to the 15 km grid of the ROMS, while in the RCM2 we linearly interpolate the original bathymetry to ~200 km grid resolution (or T62 spectral truncation) before we interpolate it to the 15 km ROMS grid. The RCM1 bathymetry had to be smoothed to avoid some numerical instability issues that arose without it. Figures 1a and 1b show the bathymetry of RCM1 and RCM2 and their differences in Figure 1c. The differences in Figure 1c are apparent in many locations including along the Atlantic coast of Florida because of the nature in which the bathymetry was prescribed in the two experiments. The point of this exercise was to make the Florida Current sufficiently different between RCM1 and RCM2 versions of the model integration. It may be noted that even for models with comparable horizontal resolution, there could be vast differences in the prescribed bathymetry as a result of the choice of the vertical coordinate in the ocean model [*Mellor et al*., 1994; *Sikiric et al*., 2009]. When the surface of the vertical coordinate of the ocean model is not aligned either with the geopotential or density surfaces, then the error in computing the horizontal pressure gradient could be aggravated. Therefore, to avoid this situation as much as possible, an optimal bathymetry for the model is chosen. In a model like ROMS that uses a terrain-following vertical coordinate system, the largest errors in horizontal pressure gradient computation happens in the presence of steep topographic gradients [*Haney*, 1991].

We analyze the results from the RCM experiments over a smaller domain with a focus on the rainy (or wet) season of PF. The emphasis of the analysis of the RCM integrations is on the terrestrial climate of PF during the wet season, which usually overlaps with the June-July-August (JJA) season. In this context, it may be noted that the observed SSTs (Optimally Interpolated SST version 2 (OISSTv2) following *Reynolds et al*. [2007]) in JJA are relatively warm, with temperatures in the range of 30°C in the Caribbean Sea (Figure 2a), which drops by a couple of degrees as we move farther north along the western subtropical Atlantic (off the eastern coast of PF). However, it is sobering to note that both RCM simulations significantly underestimate the observed SST (Figures 2b–2e). The largest differences in the climatological seasonal mean JJA SST between RCM1 and RCM2 in Figure 2f appear along the Atlantic coast of PF, which is also the location of the surface Florida Current. But the proximity to the coast, with its shallower bathymetry along PF in addition to the prevalent strong surface currents, would demand sufficient spatial and temporal resolution to resolve the variations of SST in this region. For example, the climatological SST based on the recent Met Office Operational SST and Sea Ice Analysis system (OSTIA) [*Donlon et al*., 2011] (Figure 3a), available globally at ~5 km grid spacing and at daily interval shows far more structure along the coast, over the Florida Straits than OISSTv2 (Figure 3b) and display significant differences (Figures 3d and 3e). These differences in the two different observational SST analyses arise from the use of different combinations and weights given to the satellite retrieved products and the analysis procedures, which result in such large differences [*Reynolds and Chelton*, 2010]. In addition, the OISSTv2 climatology over the available period of OSTIA SST and that over the RCM integration period (1984–2010) show considerable differences (Figures 3b, 3c, and 3f). In other words, Figure 3 strongly suggests that we need long record of high-resolution SST to validate these high-resolution RCM simulations.

Nevertheless, it is the impact of this large difference in Atlantic coastal SST along PF between RCM1 and RCM2 that we will investigate in the rest of the paper. Moreover, the global models also show similar but larger SST errors in the IAS region [*Misra et al*., 2009; *Kozar and Misra*, 2012; *Liu et al*., 2012, 2015]. It is possible that other configurations of bathymetry may have resulted in similar results, but our attempts to exclusively change the bathymetry along the Atlantic coast of Florida did not yield as large of a change in the Gulf Stream as was observed between RCM1 and RCM2. This could primarily stem from the fact that the Loop Current system in RCM1 and RCM2 are sufficiently modulated to yield the differences observed in Figure 2f. It may be noted that there are some significant differences in SST along the Gulf coast of the U.S. in Figure 2f, albeit weaker than those along the Atlantic coast of Florida. These differences in SST between the two RCM simulations in Figure 2f is consistent with previous high-resolution ocean downscaling studies of *Liu et al*. [2012, 2015] who showed that in a future warm climate, the volume transport through the Yucatan Channel would be reduced by 20–25% leading to a cooling impact (and reduced warming) over the northern Gulf of Mexico.

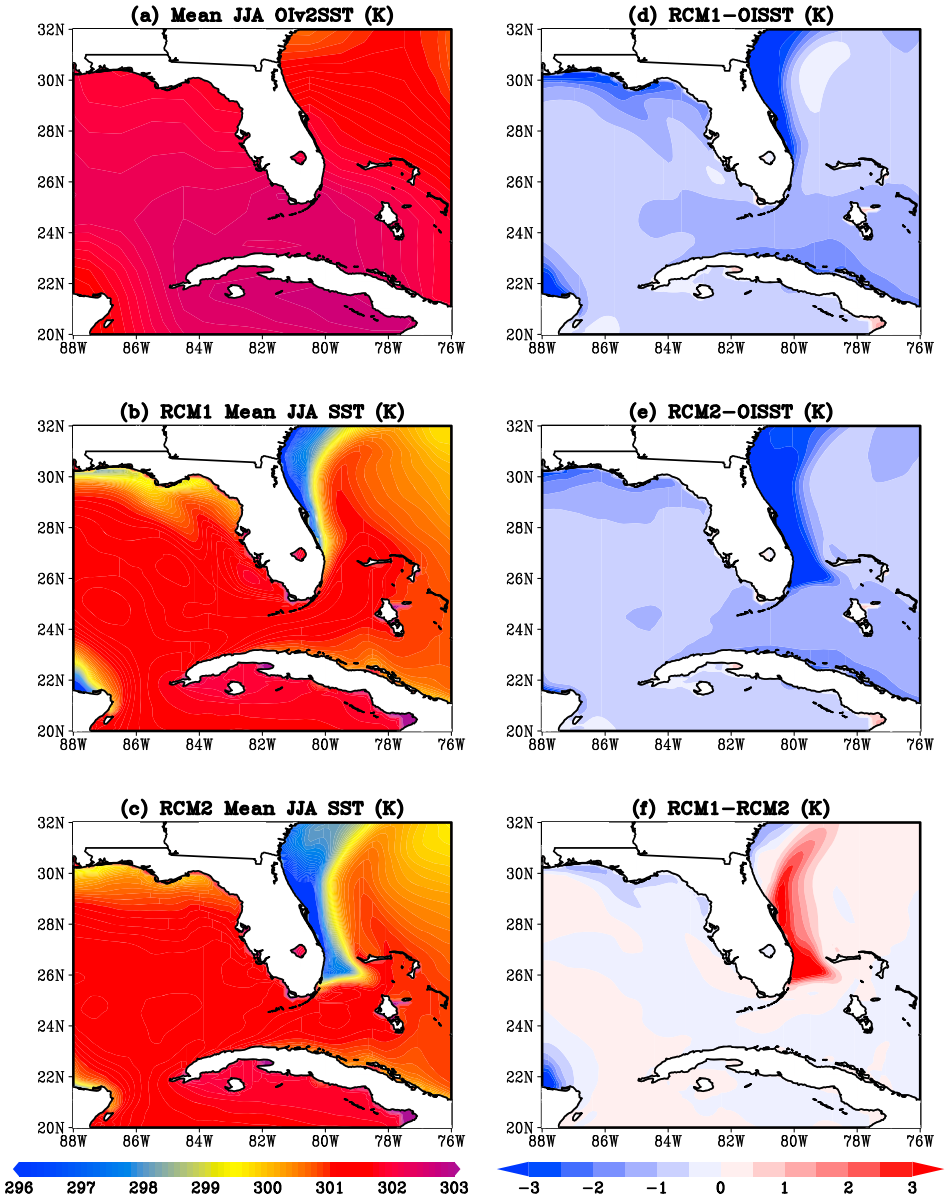

Figure 2. The climatological mean JJA SST (in K) from (a) observations (OISSTv2), (b) RCM1 integration, and (c) RCM2 integration. The corresponding systematic error (°C) of (d) RCM1 and (e) RCM2 and (f) the difference between RCM1 and RCM2.

3. Results

3.1. Wet Season Climatology

Following *Misra and DiNapoli* [2013], we define onset and demise of the wet season when the daily cumulative rainfall anomalies reach a minimum and a maximum for the year, respectively. We also additionally ensure that for a given grid point in the domain, the length of the season as determined by the difference of the date of the demise from onset is the longest and has the largest positive slope for the year. The length of the wet season climatology from observations and the two RCM integrations are shown in Figures 4a–4c, respectively. Here the observations are from NOAA's Climate Prediction Center unified gauge-based analysis of daily precipitation over land [*Xie et al*., 2007; *Chen et al*., 2008a, 2008b] available at 0.5° × 0.5° spatial resolution, globally overlapping with the 27 year period (1984–2010) of the RCM integrations.

The observations indicate a meridional gradient with south Florida exhibiting the longest wet season length of ~140 days, which gradually reduces as we move farther north along the Gulf coast of PF (Figure 4a). The

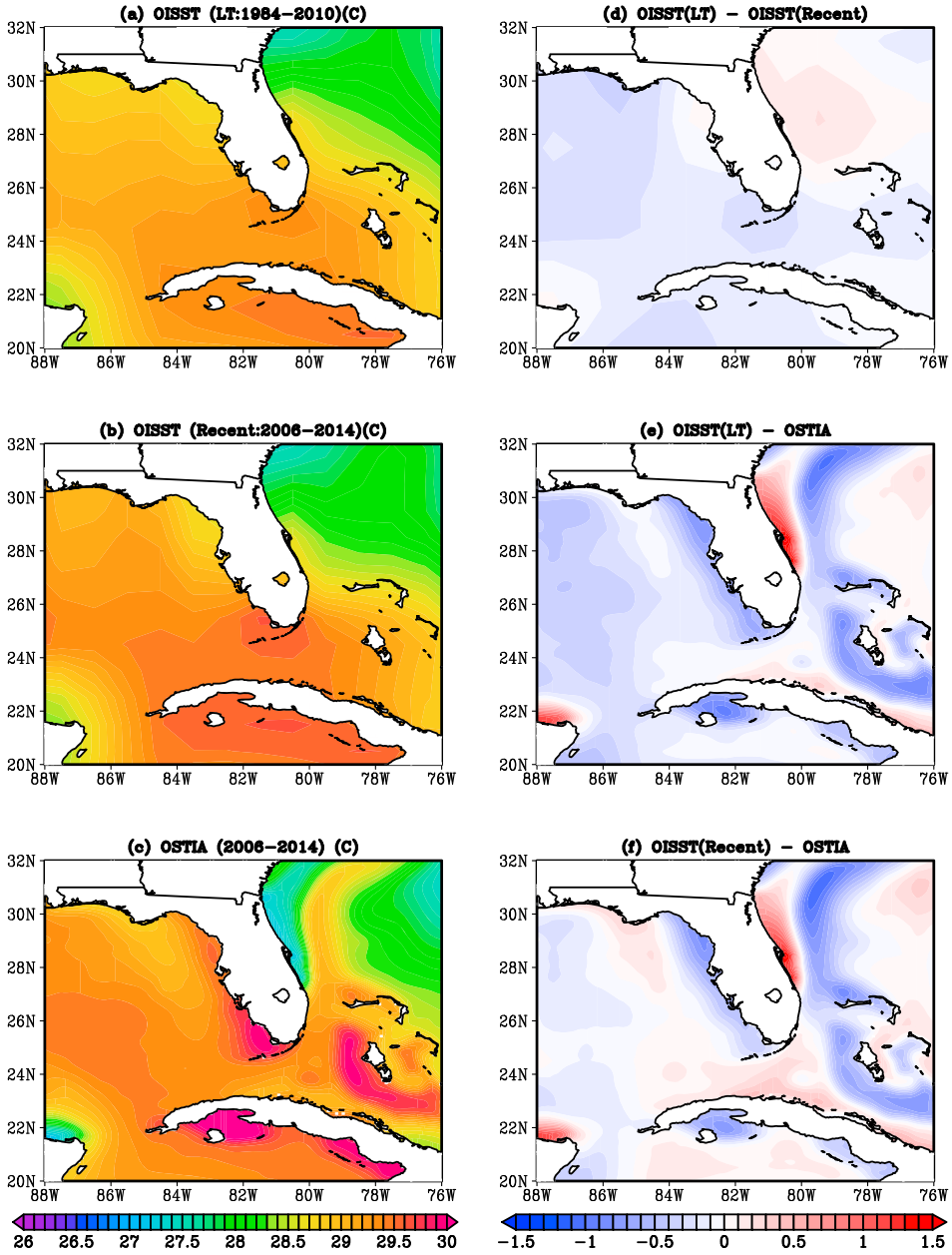

Figure 3. The climatological mean JJA SST (°C) from (a) OSTIA (climatological period is 2006–2014), (b) OISSTv2 (ST; climatological period is 2006–2014), (c) OISSTv3 (climatological period is 1984–2005), (d) Figure 3b minus Figure 3a, (e) Figure 3c minus Figure 3a, and (f) Figure 3c minus Figure 3b.

reduction in the observed seasonal length of the wet season is even more gradual along the Atlantic coast of PF. Both RCM1 (Figure 4b) and RCM2 (Figure 4c) show significant bias in this metric. But RCM1 seems to qualitatively maintain the observed meridional gradient in the seasonal length over PF far more reasonably than RCM2. In both the RCM simulations, however, south of Jacksonville in the east and south of Ft. Myers in the west display a bias of short wet season. The differences of the wet season length between RCM1 and RCM2 in Figure 4d show that RCM2 displays a shortened wet season relative to RCM1 on an average over PF by ~10 days. These differences in Figure 4d indicate that RCM2 exacerbates the bias in the length of the wet season relative to RCM1.

The observed onset date of wet season (Figure 5a) is anywhere from mid-May in south Florida to early -June in central and northern part of PF. The bias in maintaining the observed meridional gradient of the seasonal

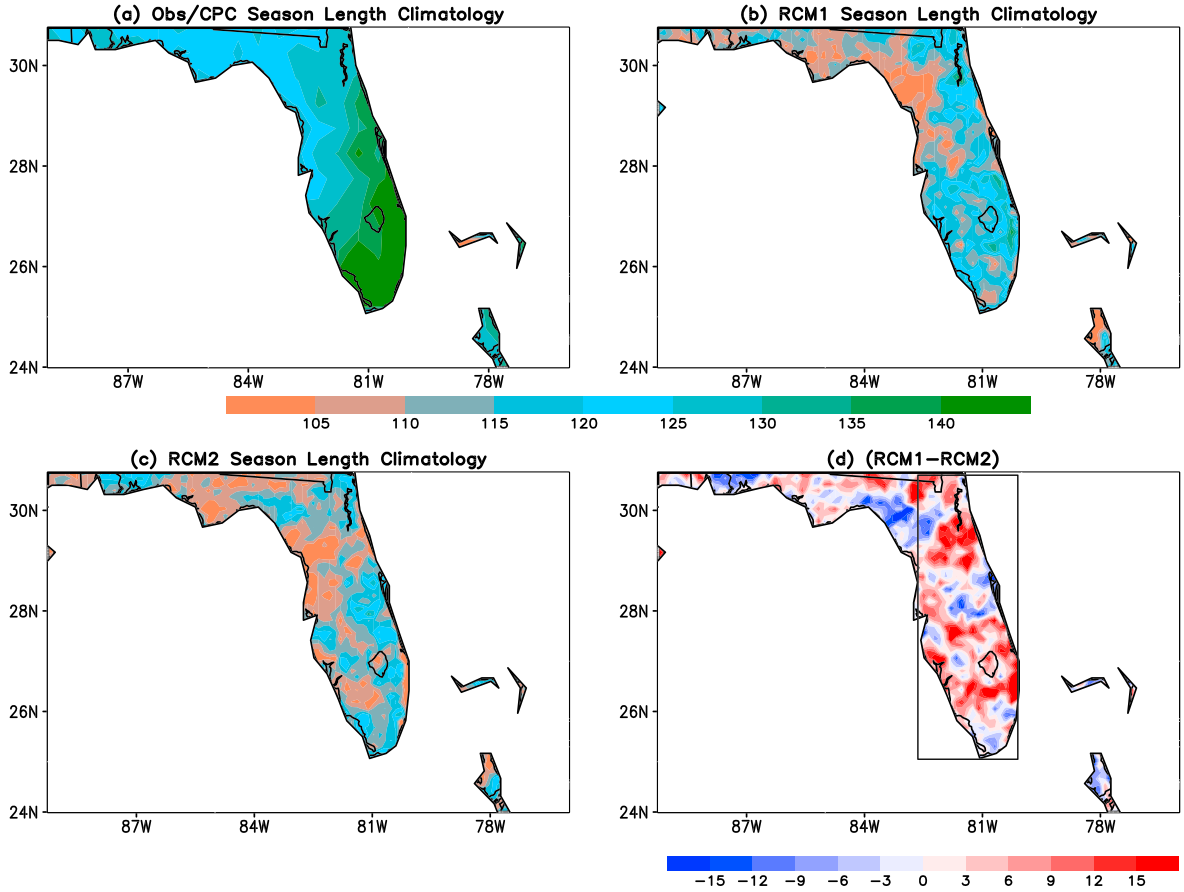

Figure 4. The climatological length of the wet season (in days) from (a) observations, (b) RCM1, (c) RCM2, and (d) RCM1 − RCM2 (Figure 4b minus Figure 4c). The outlined box in Figure 4d is showing the area (only land points enclosed in the box) over which some area average statistics are computed in Figure 6 and the hydrological budget computed in Figure 8 is based on the area average onset date of rainy season over this box.

length of the wet season in the RCM simulations seems to largely stem from the bias in the simulation of the onset dates (Figures 5b and 5c). Both models seem to display a later onset date (~10 June) over most of PF relative to the observations with an erroneously much later onset date (~25 June) in south Florida. This bias in the onset date of the wet season in the RCM simulations stem partly from the misrepresentation of the land cover type in the Everglades region as perennial ground cover [cf. *Selman and Misra*, 2015, Figure 1] as swamp or saturated land mass type does not exist in the land surface model [*Ek et al.*, 2003]. Furthermore, bias in the clouds and associated surface fluxes (not shown) and their consequent impact on bias of surface temperature, moisture flux convergence, and convection (shown later) also affect the onset date simulation in the RCM. This bias is further accentuated in RCM2 by significant bias in the surface currents around PF, shown later in the paper.

The differences between the two model simulations (Figure 5d) suggest that the reduction of the length of the wet season in RCM2 over south central PF (between latitudes of Fort Myers and Miami and east of Lake Okeechobee up to Vero Beach) largely stems from the corresponding later onset date relative to RCM1. In rest of PF, earlier demise in RCM2 is cause for the shortened length of the wet season as discussed further below.

The demise date shows a much weaker meridional gradient from south to north PF in both observations and the RCM integrations (Figures 5e–5g). Along the Atlantic coast of Florida there is nearly a continuum of late demise of the wet season displayed by both observations and model simulations. The observed demise date is approximately around 1 October averaged over PF. The differences between the two model simulations (Figure 5h) show that RCM2 has an earlier demise than RCM1 over south of Lake Okeechobee, central PF (Tampa Bay region), and northwestern PF (Jacksonville-Daytona Beach region). But over and east of Lake Okeechobee, RCM2 displays a later demise than RCM1. In summary, the longer wet season of RCM1 relative

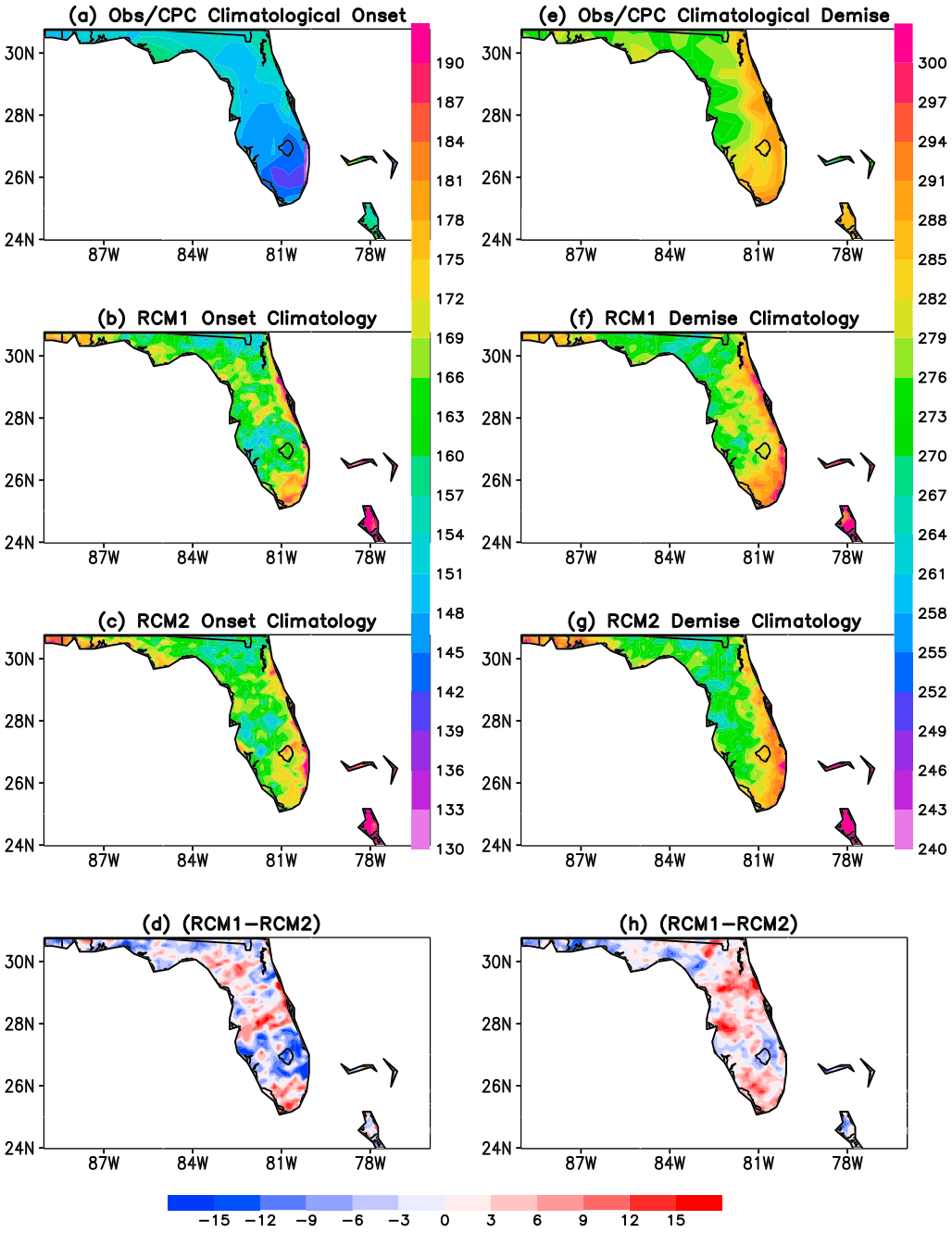

Figure 5. The climatological onset date of wet season (in Julian day) from (a) observations, (b) RCM1, (c) RCM2, and (d) RCM1 − RCM2 (Figure 5b minus Figure 5c). Similarly, the climatological demise date of wet season (in Julian day) from (e) observations, (f) RCM1, (g) RCM2, and (h) RCM1 − RCM2 (Figure 5f minus Figure 5g).

to RCM2 over PF (Figure 4d) has contributions of combinations of differences in onset and demise dates between the simulations.

The corresponding climatological seasonal accumulation of rainfall of the wet season is shown in Figures 6a–6c from observations and the two RCM integrations, respectively. It is apparent from the figure that the observed rainfall accumulation is uniformly and significantly higher (by over twice as much) than either of the two RCM simulations. But RCM2 displays a significant reduction in the seasonal accumulation of rainfall over PF relative to RCM1 (Figure 6d). This is primarily because of the corresponding reduction in the seasonal length of the wet season in RCM2 (Figure 4d). However, the daily rain rate also diminishes in intensity in RCM2 relative to

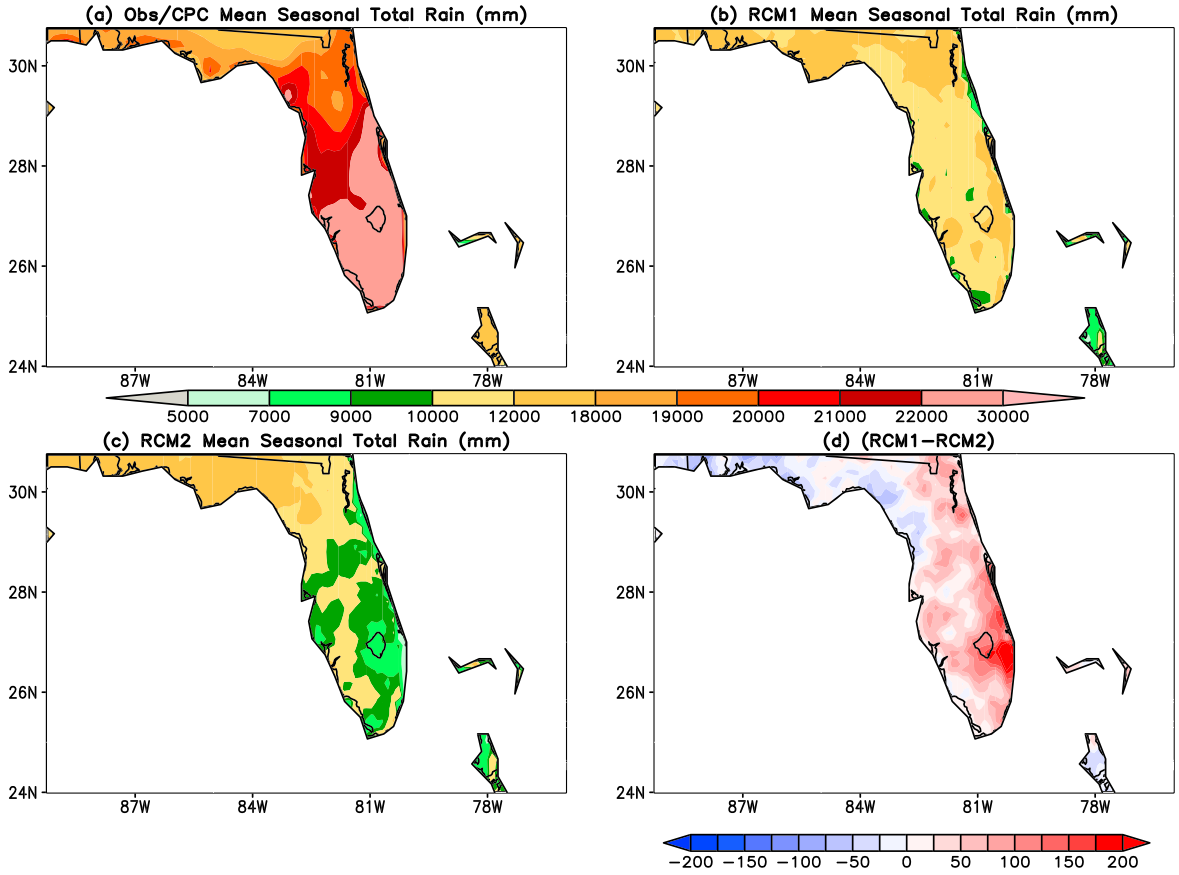

Figure 6. The climatological seasonal accumulation (in mm) during the wet season from (a) observations, (b) RCM1, (c) RCM2, and (d) RCM1 − RCM2 (Figure 6b minus Figure 6c).

RCM1. This is shown from the kurtosis (Figure 7a) and skewness (Figure 7b) for each season between the two simulations averaged over the box outlined over PF in Figure 4d. Kurtosis (K) is defined as

$$K = \frac{\sum_{i=1}^{N} \left(Y_i - \overline{Y}\right)^4 / N}{\sigma^4} \tag{1}$$

and Skewness (S) is defined by

$$S = \frac{\sum_{i=1}^{N} \left(Y_i - \overline{Y}\right)^3 / N}{\sigma^3} \tag{2}$$

where σ is the standard deviation of daily precipitation in the wet season, Y_i is the standardized daily precipitation of the wet season for a given year, $\overline{Y}$ is the sample mean (in our case seasonal mean and area averaged precipitation over PF), and N is the number of days in the wet season with i being the day of the season. A positive (negative) kurtosis would mean the peak of the distribution is sharper (flatter) and the tails are heavier (lighter). Similarly, a positive (negative) skewness would suggest that the tail right (left) of the peak is long. Both these higher-order metrics are positive for majority of the seasons in both RCM simulations. This implies in the case of skewness that the distribution of daily precipitation in the wet season is skewed toward the right (or heavier precipitation events). Likewise, the positive kurtosis (>3) would suggest that the distribution of daily precipitation is sharper than normal distribution. However, both these metrics are lower in RCM2 compared to RCM1 for majority of the seasons (Figure 7). The lower kurtosis in RCM2 suggests that its daily precipitation distribution has generally flatter peak and less heavier tail than RCM1 (Figure 7a). Similarly, the comparison of skewness in Figure 7b suggests that the daily precipitation distribution is skewed

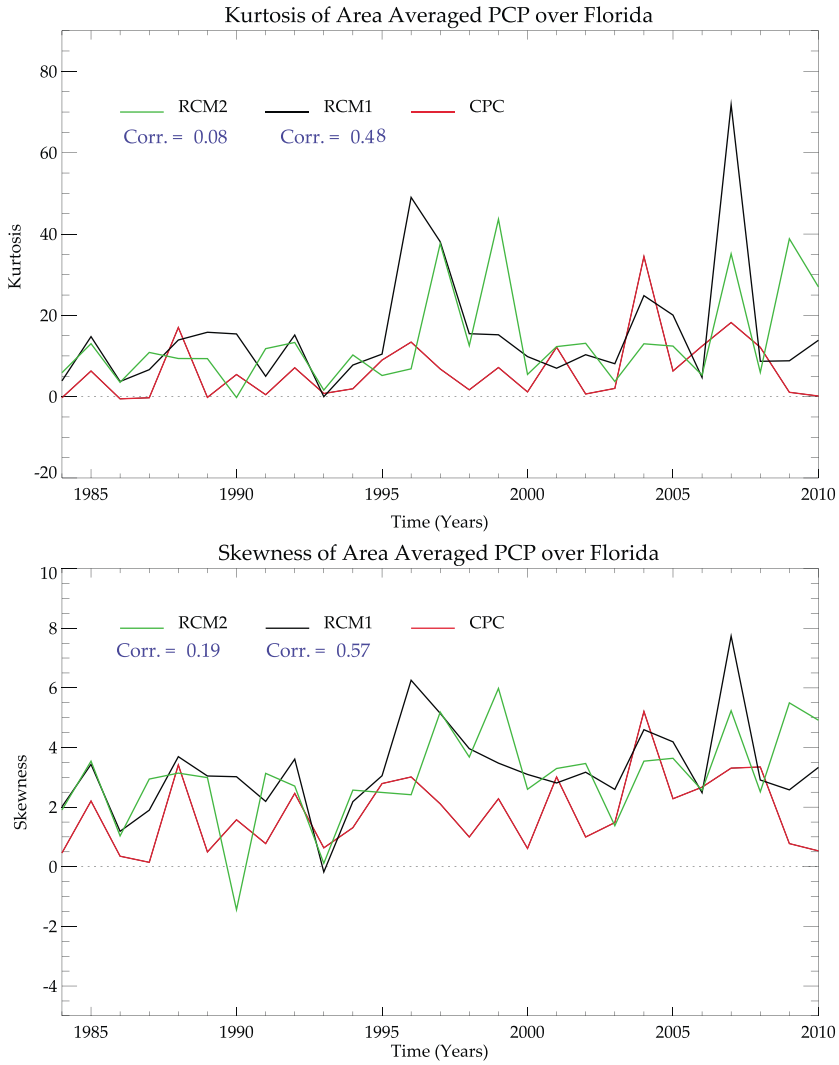

Figure 7. The (a) kurtosis and (b) skewness of daily precipitation averaged over the box outlined over peninsular Florida in Figure 4d for each wet season from the two RCM integrations and the corresponding observations (CPC). The correlations of these higher-order moments from the simulation with the corresponding observed are indicated under the respective RCM legends.

more to the left (toward lower rain rates) in RCM2 compared to RCM1 for the majority of the seasons. These figures suggest that the RCM1 has more frequent heavier precipitation in the wet season than RCM2 for majority of the years. Furthermore, it may be noted that the correlation of the observed kurtosis with corresponding values from RCM1 is significantly higher than that of RCM2 (Figure 7a). Similarly, the observed skewness with those of RCM1 is also very high compared to that with RCM1 (Figure 7b). Both of these suggest that the distribution of daily rainfall during the wet season is far more well represented in RCM1 compared to RCM2.

3.2. The Moisture Budget

In order to understand the differences between the RCM simulations shown in the previous subsection we compute the atmospheric moisture budget. The vertically integrated atmospheric moisture budget is given by

$$\frac{\partial Q}{\partial t} = \varpi + E - P \tag{3}$$

where Q is precipitable water and is given by

$$Q = \int_{p_{bot}}^{p_{top}} q \frac{dp}{g} \tag{4}$$

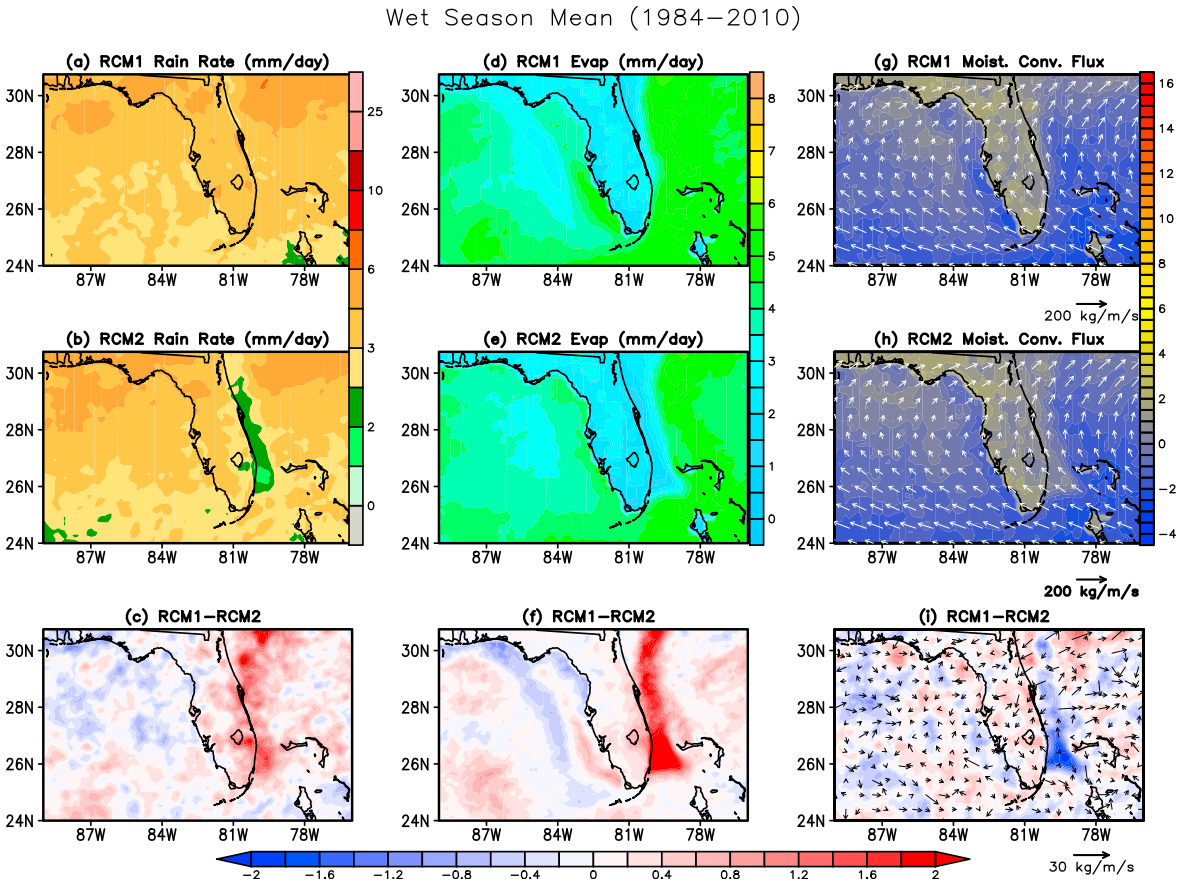

Figure 8. The climatological mean rain rate (mm d^{-1}) from (a) RCM1, (b) RCM2, (c) RCM1 − RCM2 (Figure 8a minus Figure 8b) averaged over the length of the wet season. Similarly, the climatological mean surface evaporation rate (mm d^{-1}) from (d) RCM1, (e) RCM2, (f) RCM1 − RCM2 (Figure 8d minus Figure 8e) averaged over the length of the wet season. Likewise the climatological mean moisture flux convergence rate (mm d^{-1}) overlaid with moisture flux vectors (kg m^{-1} s^{-1}) averaged over the length of the season from (g) RCM1, (h) RCM2, and (i) RCM1 − RCM2 (Figure 8g minus Figure 8h).

where q is specific humidity, E and P are surface evaporation and precipitation rate, and ϖ is moisture flux convergence given by

$$\varpi = -\int_{p_{bot}}^{p_{top}} \nabla \cdot \vec{V}\, q \frac{dp}{g} \tag{5}$$

It may be noted that positive (negative) values of ϖ correspond to moisture flux convergence (divergence). We will focus on the moisture budget terms in equation (3), averaged over the wet season from their corresponding daily values. In both RCM simulations the rain rate over PF (south of Gainesville) is relatively higher than the neighboring oceans (Figures 8a and 8b). In RCM2 the terrestrial rain rate over PF and as well as over the Florida Current east of Florida is lower than RCM1 (Figure 8c). The terrestrial surface evaporation, however, is lower than that over the surrounding oceans in both RCM simulations (Figures 8d and 8e). The differences in Figure 8f indicate that RCM2 evaporates slightly less moisture than RCM1 over PF but significantly less over the coastal Florida Current region. Some of these differences between the two model simulations could be related to local precipitation recycling, which makes it difficult to discern the cause and effect between precipitation and evaporation. Nonetheless, increased evaporation in the coastal ocean feeds in to terrestrial hydrological cycle over PF [*Misra and DiNapoli*, 2013; *Chan and Misra*, 2010]. This is further confirmed by the comparison of the moisture flux convergence and moisture flux vectors from the two RCM simulations (Figures 8g–8i). We find that both models show generally a stronger moisture flux convergence over PF and either weak moisture flux convergence or moisture flux divergence over the neighboring warm tropical and subtropical oceans, with southwesterly (southeasterly) moisture flux vectors over south (north) PF. Again, we note that RCM2 has comparatively less moisture flux convergence over PF

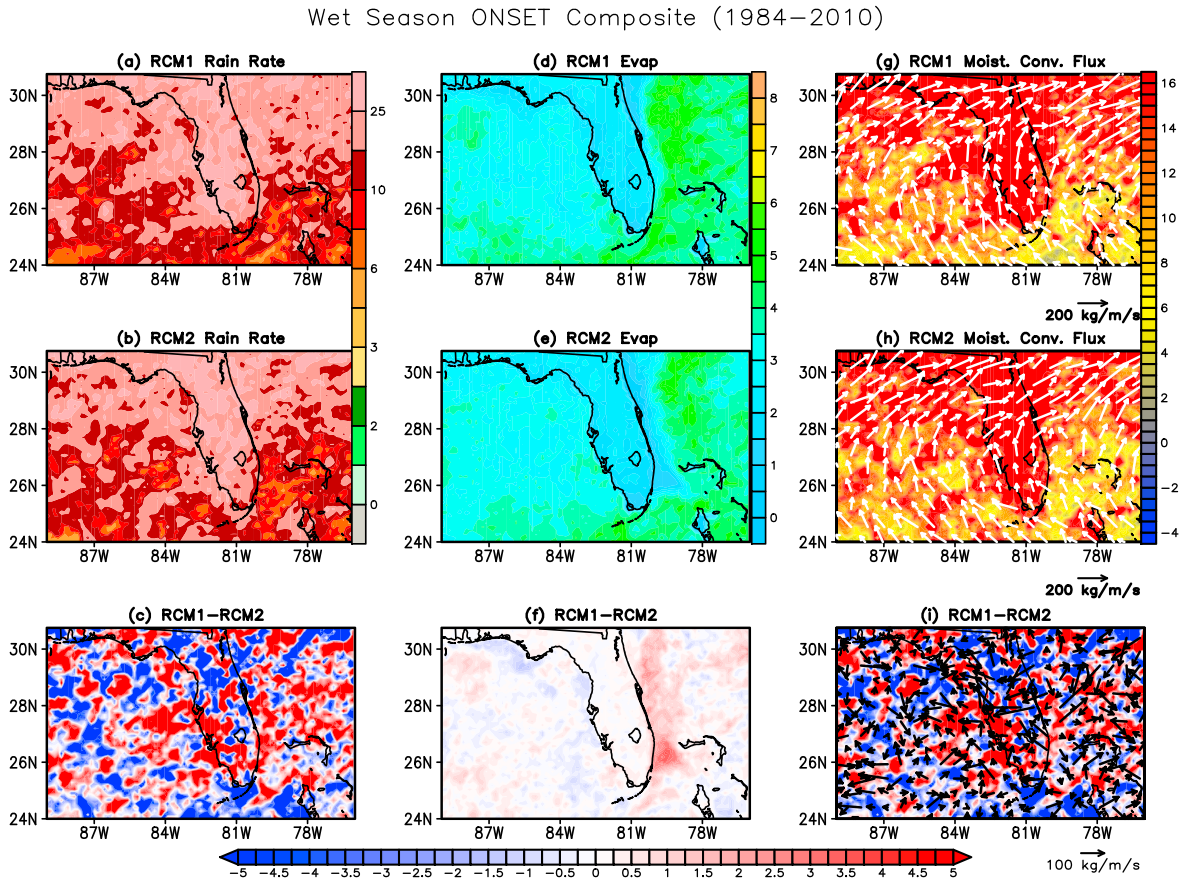

Figure 9. The climatological mean rain rate (mm d^{-1}) from (a) RCM1, (b) RCM2, (c) RCM1 − RCM2 (Figure 9a minus Figure 9b) for the day of onset of the wet season for the box outlined over peninsular Florida in Figure 4d. Similarly, the climatological mean surface evaporation rate (mm d^{-1}) from (d) RCM1, (e) RCM2, (f) RCM1 − RCM2 (Figure 9d minus Figure 9e) for the day of onset of wet season over peninsular Florida. Likewise the climatological mean moisture flux convergence rate (mm d^{-1}) overlaid with moisture flux vectors (kg m^{-1} s^{-1}) for the day of onset of wet season over peninsular Florida from (g) RCM1, (h) RCM2, and (i) RCM1 − RCM2 (Figure 9g minus Figure 9h).

than RCM1 (Figures 8h and 8i). The differences between the two model simulations in Figure 8i indicate that in addition to lower moisture flux convergence over PF, RCM2 also exhibits less moisture flux divergence over the Florida Current to the east of South Florida compared to RCM1. In addition, the moisture flux vectors in Figure 8i also indicate that oceanic source of moisture is reduced over PF in RCM2 relative to RCM1.

Similar to Figure 8, we have plotted the composite of the moisture budget at the time of onset of the wet season for the two RCM simulations in Figure 9. We see that the rain rate over PF increases from Tampa to Naples and along Tampa-Orlando corridor in RCM1 compared to RCM2 (Figures 9a–9c). But differences in terrestrial surface evaporation over PF at the time of the onset of the wet season between the simulations are negligible (Figures 9d–9f). However, along the Atlantic coast of PF the surface evaporation is over 3 mm d^{-1} in RCM1 compared to RCM2 (Figure 9f). The moisture flux convergence in Figures 9g–9i reveal that the increases in rain rate noted in RCM1 (Figure 9c) coincides with similar increase in moisture flux convergence relative to RCM2 (Figure 9i). The moisture flux vectors also show a decrease in moisture from the ocean to PF in RCM2 relative to RCM1 (Figures 9g–9i). Similarly, the decrease in the rain rate north of the Tampa-Orlando corridor and over southern tip of PF (Figure 9c) is associated with similar decrease in the moisture flux convergence in RCM1 compared to RCM2 (Figure 9i). It may also be noted that the magnitude of moisture flux convergence and rain rate in Figure 9 is much higher than in Figure 8 because the former is a composite for a day while the latter is an average over a season. We observe similar features of the moisture budget terms in the RCM simulations at time of demise of the wet season as the onset date (not shown).

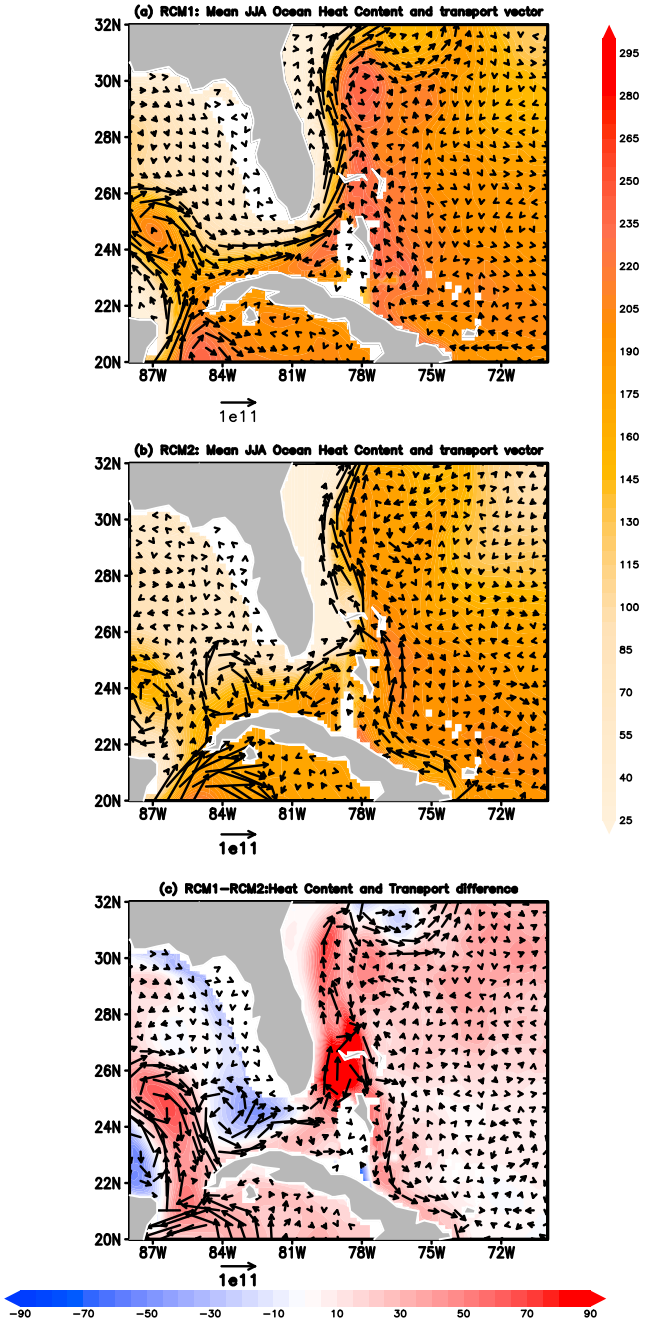

Figure 10. The climatological mean JJA ocean heat content as measured by the depth of the 20°C isotherm (in meters) overlaid with upper ocean heat transport vectors (equation 5 in text; W m^{-1}) from (a) RCM1, (b) RCM2, and (c) RCM1 − RCM2 (Figure 10a minus Figure 10b).

In summary the moisture budget reveals that the relative reduction of warm season precipitation in RCM2 over PF is associated with a decrease in evaporation over the warm Florida Current (along the Atlantic coast of PF) and the consequent reduction in moisture flux convergence to feed convection in the terrestrial PF region. It should also be noted that both at the time of the onset (Figure 9) and demise (not shown) of the rainy season, the differences in surface evaporation (moisture flux convergence) over PF between the two RCM simulations are insignificant (significant). Thus, we can conclude that a combination of reduced season length and daily rain rate over the season in RCM2 leads to an overall weaker rainy season relative to RCM1.

3.3. Ocean Circulation and Heat Content

So far we have clearly shown that by changing the prescribed bathymetry for the ocean component of the RCM modulates the wet season precipitation over PF. The RCM that displays colder SST off the Atlantic coast of Florida shows shorter wet season and lower seasonal accumulation of rainfall. This reduction of SST off the Atlantic coast of PF in RCM2 relative to RCM1 is sustained by the corresponding lower ocean heat content as measured by the depth of the 20°C isotherm (Figures 10a–10c). In turn, this relative cooling of the upper ocean is primarily dictated by the weaker ocean heat transport from the warmer Caribbean Sea to the subtropical Atlantic Ocean through the Loop and Florida Current [*Liu et al.*, 2012, 2015]. The upper ocean heat transport between the surface and the depth of the 20°C isotherm is given by the following equation:

$$\vec{H} = \int_{Z_{20C}}^{Z_{surface}} \vec{V}\, TC_w\rho_w dz \qquad (6)$$

where $\vec{V}$ is the ocean current, T is the ocean temperature, C_w and ρ_w are heat capacity and density of sea water, and Z_{20C} is the depth of the 20°C isotherm. The depth of the 20°C isotherm marks approximately the boundary between the warmer upper ocean and colder (and denser) deep ocean in the tropical and subtropical latitudes [*Kessler*, 1990]. Since the Florida and Loop Currents are surface currents, they largely affect the upper ocean heat content, which is the reason for integrating equation (6) to a depth of 20°C isotherm from the surface. These ocean heat transport vectors in Figures 10a–10c clearly show the reduction in the heat transport in RCM2 relative to RCM1 that leads to the systematic decrease in ocean heat content of

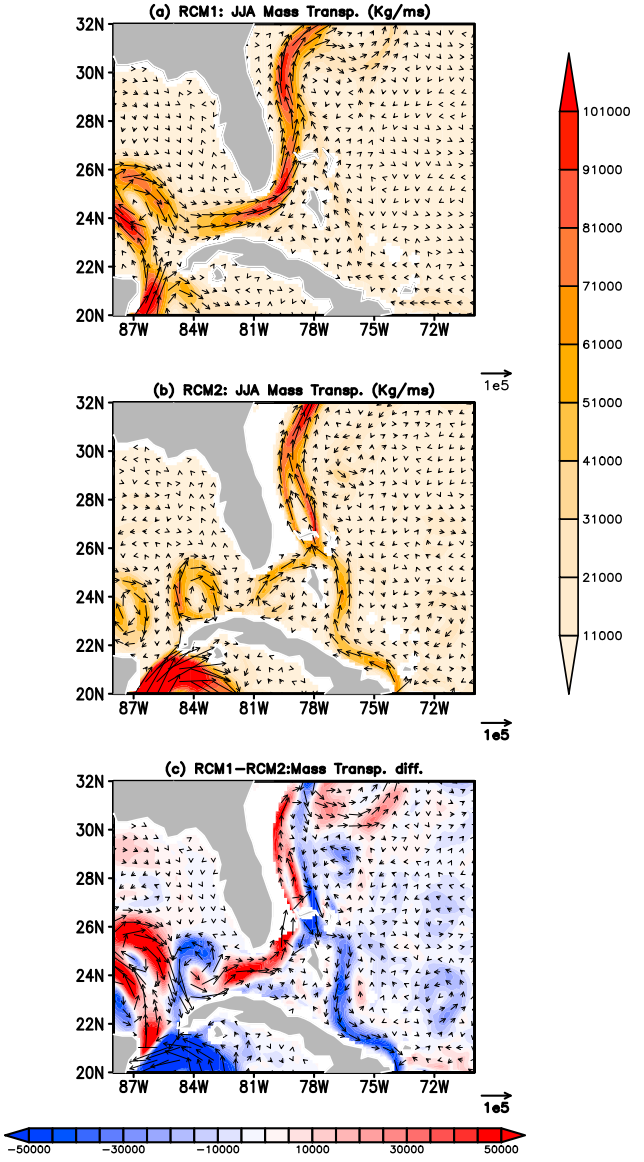

Figure 11. The climatological mean JJA ocean mass transport vectors (magnitude is shaded; kg m^{-1} s^{-1}) from (a) RCM1, (b) RCM2, and (c) Figure 11a minus Figure 11b.

the former compared to the latter. That this reduction in heat transport is largely dictated by reduction in the mass transport is indicated in Figure 11, which shows the mass transport vectors $\left(\vec{M}\right)$ following equation (7) given below:

$$\vec{M} = \int_{Z_{20C}}^{Z_{surface}} \vec{V}\, \rho_w dz \qquad (7)$$

It is clear from Figure 11 that the Loop and the Florida Currents are considerably weaker in RCM2 compared to RCM1.

4. Discussion

In this section we discuss a mechanistic view to the results discussed thus far, which shows that neighboring oceans have a subtle influence on the wet season of PF. This is shown schematically in Figure 12. The prescribed bathymetry in a RCM dictates the ocean circulation and its heat transport vectors, which ultimately manifest in the modulation of the upper ocean heat content. The western intensification of subtropical gyres that results in the warm surface boundary current along the eastern U.S. seaboard stems from simple mass and potential vorticity conservation, better known by the Sverdrup relationship [*Stommel*, 1948]. The prescribed bathymetry has a central role to play as it dictates the depth of the water column, which ultimately affects the mass and potential vorticity. In addition, the prescribed bathymetry is also affecting the inflow through the channels in the region (e.g., Florida Straits and Yucatan Channel) that also affects the upper ocean heat transport and the SSTs along the western Atlantic coast. For example, in RCM2 the coarser bathymetry restricted the flow through the Yucatan Channel and Florida Straits, which diminished the heat transport from the Caribbean Sea through the Gulf of Mexico to the subtropical northwestern Atlantic Ocean. This resulted in significantly cooling the SST over the Florida Current region (off the Atlantic coast of Florida) in RCM2 relative to RCM1. As a result the evaporation off the warm surface over the Florida Current reduced and in turn there was less moisture flux convergence over PF in RCM2. This resulted in delayed onset and early demise in various regions of PF resulting in an overall reduction in the length of the wet season in RCM2 simulation. This consequently led to reduced seasonal mean rain rate through the relatively short wet season in RCM2 relative to RCM1. The results of this study are consistent with the findings of *Liu et al*. [2012, 2015], which also showed that reducing the mass transport through the Yucatan Channel in a future warming climate leads to cooling in the IAS.

Moisture flux convergence is the dominating influence on rainfall at time of onset and demise. Surface evaporation plays a far less influential role on rainfall modulation at the time of onset of the wet season. This is consistent with the fact that the onset happens from a relatively prior dry (spring) season resulting in drier soil

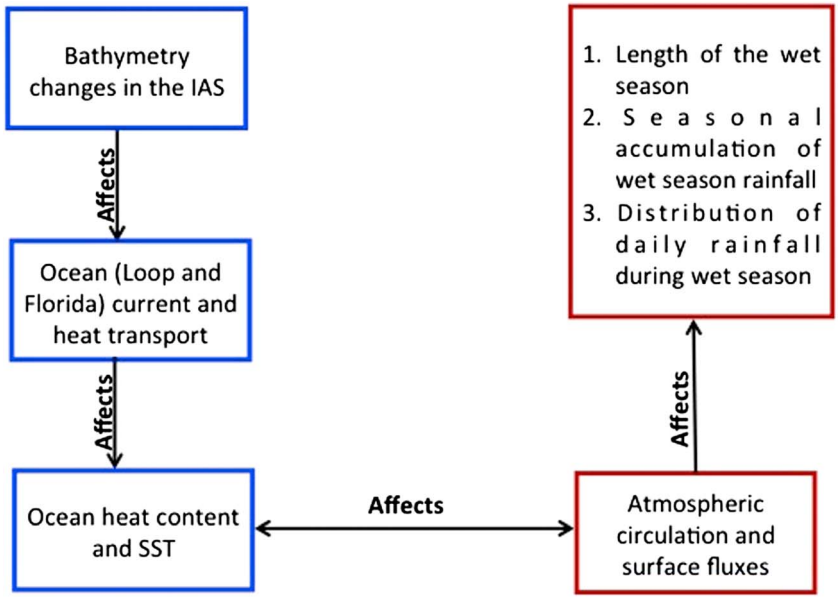

Figure 12. The schematic of the ocean feedback mechanism affecting wet season rainfall over peninsular Florida. The boxes outlined in blue (brown) refer to oceanic (terrestrial) variables.

moisture conditions than in the midst of the wet season. Similarly, at time of demise the rain rates begin to subside from the seasonal peak substantially, resulting in far less contribution from precipitation recycling (not shown). So in RCM2 on account of diminished surface evaporation off the Atlantic coast of Florida there is less moisture flux convergence over PF resulting in a later onset and or early demise of the wet season (Figures 8 and 9). It may be noted that the differences in rainfall between RCM1 and RCM2 over PF are comparatively less extensive over PF when examined over the average JJA season than shown in Figure 6d or Figure 8c because such an average does not take into account the modulation of the length of the season (Figure 13). For example, even the spatial structure of the observed climatological wet season rain over PF in Figure 13a is different from the corresponding mean in Figure 6a averaged over a varying length of the wet season. Similarly, the differences between RCM1 and RCM2 in Figure 13d are less extensive relative to Figure 6d, like the positive differences north of Lake Okeechobee is weak in the JJA mean differences. Therefore, accounting for the changes in the length of wet season is an important component to assess when analyzing the impact on the hydroclimate of PF from changes in the surrounding ocean surface currents.

5. Conclusions

This paper highlights the difference in the simulation of the regional terrestrial climate over Peninsular Florida arising from the placement and strength of the ocean currents in the vicinity of Florida's coastline. The RCM experiments clearly suggest that large changes in western Atlantic coastal upper ocean heat content can be affected by changes to bathymetry. The changes to the upper ocean heat content impacts the local surface evaporation and convection over the warm waters overlying the Florida Current off the Atlantic coast of PF. In turn this affects the magnitude and timing of the moisture flux convergence over PF, which manifests in changes to the onset and demise date and the magnitude of the rain rate of the wet season. Another aspect that is highlighted from these RCM experiments is that with identical model grid resolution, one could affect the simulation of the seemingly grid resolution dependent features (e.g., surface ocean currents and coastal rainfall) by changes in bathymetry.

These results are instructive to interpret changes in wet season rainfall over PF from large-scale changes to the coastal SST. After all, Florida Current along the Atlantic coast is part of the western boundary current and the Atlantic meridional overturning circulation, which manifests from the western intensification of the large-scale Atlantic subtropical gyre [*Stommel*, 1948]. These large-scale features can also change from natural variations or from anthropogenic influence or a combination of the two [*Wang et al*., 2010; *Zhang*

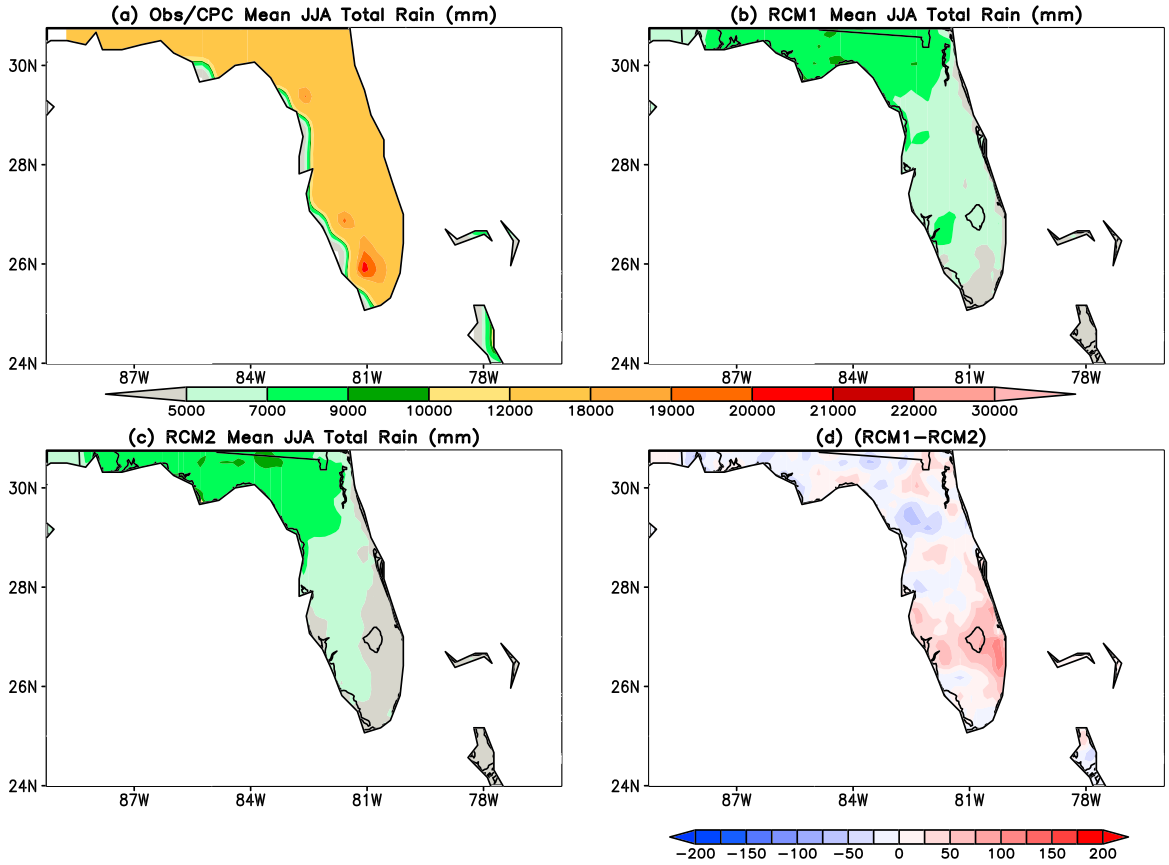

Figure 13. The climatological seasonal accumulation (in mm) for a fixed length of June-July-August (JJA) season from (a) observations, (b) RCM1, (c) RCM2, and (d) RCM1 − RCM2 (Figure 13b minus Figure 13c).

et al., 2014], which this study would suggest could have an implication on the wet season rainfall over PF. Furthermore, we highlight the importance of prescribed bathymetry in climate models and encourage a closer look at the fidelity of the ocean circulations and heat content in the neighboring oceans of Florida for their potential impact on the terrestrial climate of PF. In addition, the errors in the simulation of the mesoscale surface ocean currents of the Loop and the Florida Currents could also arise from inadequate spatial grid resolution of the climate models [*Hurlburt and Thompson*, 1980; *Chérubin et al*., 2005, 2006], inappropriate choice of bathymetry and or vertical discretization of the model [*Mellor et al*., 1994; *Sikiric et al*., 2009]. For a region like Florida, which receives most of its total annual rainfall in the summer season, such impacts of oceanic influence are notably important.

This study highlighting the impact of local processes on terrestrial rainfall over PF sheds a cautionary note on some of the earlier studies that allude to drying of the subtropical regions including Florida to warming of remote tropical ocean SSTs due to global warming [*Neelin et al*., 2003; *Xie et al*., 2010; *Rauscher et al*., 2011]. These studies were conducted with relatively coarse resolution global models that did not discuss the fidelity of the simulation of the local surface currents around PF nor indicated the fidelity of the coastal SST anomalies. It is, however, plausible to suggest from the results of this study that the weakening of these surface currents (e.g., the Loop and the Florida Currents) as part of the general weakening of the AMOC in the current [*Bryden et al*., 2005] and future [*Cheng et al*., 2013] warming climate could result in further reduction of wet season rainfall over PF.

The RCMs of this study underestimate the rainfall significantly during the rainy season over PF, which we believe is partly associated with the cold SST bias, incorrect representation of land surface type over the Everglades, and erroneous cloud simulations in the model. Despite more heat transport to the subtropical oceans from the warmer tropical oceans in RCM1 from an improved bathymetry compared to RCM2, it

continues to display a cold bias, albeit slightly weaker than in RCM2. There are other potential reasons for this bias in RCM1 including the fact that the tropical ocean is not warm enough. From the analysis of this study we conclude that improving the rainy season simulation over PF is associated with improving this cold SST bias over the neighboring ocean, which seems to be pervasive across many models [*Misra et al*., 2009; *Kozar and Misra*, 2012; *Liu et al*., 2012, 2015].

Acknowledgments
This work was supported by grants from NOAA (NA12OAR4310078 and NA11OAR4310110) and USGS G13AC00408. The supercomputing facility provided by XSEDE under grant ATM10010 was used to complete the model integrations used in this study. Data used in this study are freely available upon request from the authors via vmisra@fsu.edu.

References

Alpert, J. C., M. Kanamitsu, P. M. Caplan, J. G. Sela, G. White, and E. Kalnay (1988), Mountain induced gravity wave drag parameterization in the NMC medium-range model, in *Eighth Conference on Numerical Weather Prediction*, pp. 726–733, Am. Meteorol. Soc., Baltimore, Md, Preprints.

Bastola, S., and V. Misra (2013), Sensitivity of hydrological simulations of Southeastern United States watersheds to temporal aggregation of rainfall, *J. Hydrometeorol.*, *14*, 1334–1344.

Black, E., J. M. Slingo, and K. R. Sperber (2003), An observational study of the relationship between excessively strong short rains in coastal East Africa and Indian Ocean SST, *Mon. Weather Rev.*, *131*, 74–94, doi:10.1175/1520-0493(2003)131<0074:AOSOTR>2.0.CO;2.

Blanchard, D. O., and R. E. López (1985), Spatial patterns of convection in south Florida, *Mon. Weather Rev.*, *113*(8), 1282–1299.

Bright, R. J., L. Xie, and L. J. Pietrafesa (2002), Evidence of the Gulf Stream's influence on tropical cyclone intensity, *Geophys. Res. Lett.*, *29*(16), 1801, doi:10.1029/2002/GL14920.

Bryden, H. L., H. R. Longworth, and S. A. Cunningham (2005), Slowing of the Atlantic meridional overturning circulation at 25°N, *Nature*, *438*, 655–657.

Burpee, R. W., and L. N. Lahiffi (1984), Area-average rainfall variations on sea-breeze days in south Florida, *Mon. Weather Rev.*, *112*(3), 520–534.

Cameron-Devitt, S. E., J. R. Seavey, S. Claytor, T. Hoctor, M. Main, O. Mbuya, R. Noss, and C. Rainyn (2011), Florida Biodiversity under a changing climate. [Available at http://floridaclimate.org/biodiversity_pdf.php.]

Candela, J., S. Tanahara, M. Crepon, B. Barnier, and J. Sheinbaum (2003), Yucatan Channel flow: Observations versus CLIPPER ATL6 and MERCATOR PAM models, *J. Geophys. Res.*, *108*(C12), 3385, doi:10.1029/2003JC001961.

Carton, J. A., and B. S. Giese (2008), A reanalysis of ocean climate using simple ocean data assimilation (SODA), *Mon. Weather Rev.*, *136*, 2999–3017, doi:10.1175/2007MWR1978.1.

Chan, S., and V. Misra (2010), A diagnosis of the 1979–2005 extreme rainfall events in the southeastern United States with isentropic moisture tracing, *Mon. Weather Rev.*, *138*, 1172–1185.

Chen, M., W. Shi, P. Xie, V. B. S. Silva, V. E. Kousky, R. W. Higgins, and J. E. Janowiak (2008a), Assessing objective techniques for gauge based analyses of global daily precipitation, *J. Geophys. Res.*, *113*, D04110, doi:10.1029/2007JD009132.

Chen, M., et al. (2008b), CPC unified gauge based analysis of global daily precipitation,Western Pacific Geophysics Meeting, Cairns, Australia, 29 July–1 Aug.

Cheng, W., J. C. H. Chiang, and D. Zhang (2013), Atlantic Meridional Overturning Circulation (AMOC) in CMIP5 models: RCP and historical simulations, *J. Clim.*, *26*, 7187–7197.

Chérubin, L. M., W. Sturges, and E. P. Chassignet (2005), Deep flow variability in the vicinity of the Yucatan Straits from a high-resolution MICOM simulation, *J. Geophys. Res.*, *110*, C04009, doi:10.1029/2004JC002280.

Chérubin, L. M., Y. Morel, and E. P. Chassignet (2006), Loop current ring shedding: The formation of cyclones and the effect of topography, *J. Phys. Oceanogr.*, *36*, 569–591.

Chou, M.-D., and K.-T. Lee (1996), Parameterizations for the absorption of solar radiation by water vapor and ozone, *J. Atmos. Sci.*, *53*, 1203–1208, doi:10.1175/1520-0469(1996)053<1203:PFTAOS>2.0.CO;2.

Chou, M.-D., and M. J. Suarez (1994), *An Efficient Thermal Infrared Radiation Parameterization for Use in General Circulation Models*, *Tech. Rep. Ser. on Global model. and data Assimilation, NASA/TM-1994-104606*, vol. 3, 85 pp., NASA, Greenbelt, Md.

Cutter, S. L., and C. T. Emrich (2006), Moral hazard, social catastrophe: The changing face of vulnerability along the hurricane coasts, *Ann. Am. Acad. Polit. Soc. Sci.*, *604*(1), 102–112.

DeMaria, M., C. R. Sampson, J. A. Knaff, and K. D. Musgrave (2014), Is tropical cyclone intensity guidance improving? *Bull. Am. Meteorol. Soc.*, *95*, 387–398, doi:10.1175/BAMS-D-12-00240.1.

DiNapoli, S., and V. Misra (2012), Reconstructing the 20th century high-resolution climate of the southeastern United States, *J. Geophys. Res.*, *117*, D19113, doi:10.1029/2012JD018303.

Donlon, C. J., M. Martin, J. D. Stark, J. Roberts-Jones, E. Fiedler, and W. Wimmer (2011), The Operational Sea Surface Temperature and Sea Ice analysis (OSTIA), *Remote Sens. Environ.*, doi:10.1016/j.rse.2010.10.0172011.

Ek, M. B., K. E. Mitchell, Y. Lin, E. Rogers, P. Grunmann, V. Koren, G. Gayno, and J. D. Tarpley (2003), Implementation of Noah land surface model advances in the National Centers for Environmental Prediction operational mesoscale Eta model, *J. Geophys. Res.*, *108*(D22), 8851, doi:10.1029/2002JD003296.

Erfani, E., and D. Mitchell (2014), A partial mechanistic understanding of the North American monsoon, *J. Geophys. Res. Atmos.*, *119*, 13,096–13,115, doi:10.1002/2014JD022038.

Gordon, A. (1967), Circulation of the Caribbean Sea, *J. Geophys. Res.*, *72*, 6207–6223, doi:10.1029/jz072i024p06207.

Haidvogel, D. B., H. G. Arango, K. Hedstrom, A. Beckmann, P. MalanotteRizzoli, and A. F. Shchepetkin (2000), Model evaluation experiments in the North Atlantic Basin: Simulations in nonlinear terrain-following coordinates, *Dyn. Atmos. Oceans*, *32*, 239–281.

Haney, R. L. (1991), On the pressure gradient force over steep bathymetry in sigma coordinates ocean models, *J. Phys. Oceanogr.*, *21*, 610–619.

Hong, S. Y., and H. L. Pan (1996), Nonlocal boundary layer vertical diffusion in a medium–range forecast model, *Mon. Weather Rev.*, *124*, 2322–2339, doi:10.1175/1520-0493(1996)124<2322:NBLVDI>2.0.CO;2.

Hurlburt, H. E., and J. D. Thompson (1980), A numerical study of Loop Current intrusions and eddy shedding, *J. Phys. Oceanogr.*, *10*, 1611–1651, doi:10.1175/1520-0485(1980)010<1611:ANSOLC>2.0.CO;2.

Juang, H. M. H., and M. Kanamitsu (1994), The NMC nested regional spectral model, *Mon. Weather Rev.*, *122*, 3–26.

Kanamaru, H., and M. Kanamitsu (2007), Scale selective bias correction in a downscaling of global analysis using a regional model, *Mon. Weather Rev.*, *135*, 334–350.

Kanamitsu, M., W. Ebisuzaki, J. Wollen, S. K. Yang, J. J. Hnilo, M. Fiorino, and G. L. Potter (2002), NCEP-DOE AMIP-II reanalysis, *Bull. Am. Meteorol. Soc.*, *83*, 1631–1643.

Kanamitsu, M., K. Yoshimura, Y. Yhang, and S. Hong (2010), Errors of interannual variability and multi-decadal trend in dynamical regional climate downscaling and its corrections, *J. Geophys. Res.*, *115*, D17115, doi:10.1029/2009JD013511.

Kessler, W. S. (1990), Observations of long Rossby waves in the northern tropical Pacific, *J. Geophys. Res.*, *95*, 5183–5217, doi:10.1029/JC095iC04p05183.
Knight, D. B., and R. E. Davis (2009), Contribution of tropical cyclones to extreme rainfall events in the Southeastern United States, *J. Geophys. Res.*, *114*, D23102, doi:10.1029/2009JD012511.
Kozar, M., and V. Misra (2012), Evaluation of twentieth-century Atlantic warm pool simulations in historical CMIP5 runs, *Clim. Dyn.*, doi:10.1007/s00382-012-1604-9.
Large, W. G., J. C. McWilliams, and S. C. Doney (1994), Oceanic vertical mixing: A review and a model with a nonlocal boundary layer parameterization, *Rev. Geophys.*, *32*, 363–403, doi:10.1029/94RG01872.
Larson, J., Y. Zhou, and R. W. Higgins (2005), Characteristics of landfalling tropical cyclones in the United States and Mexico: Climatology and interannual variability, *J. Clim.*, *18*, 1247–1261.
Li, H., and V. Misra (2014), Thirty-two year ocean-atmosphere coupled downscaling of global reanalysis over the Intra-American Seas, *Clim. Dyn.*, *43*(9), 2471–2489, doi:10.1007/s00382-014-2069-9.
Li, H., M. Kanamitsu, and S. Y. Hong (2012), California reanalysis downscaling at 10 km using an ocean-atmosphere coupled regional model system, *J. Geophys. Res.*, *117*, D12118, doi:10.1029/2011JD017372.
Li, H., M. Kanamitsu, S. -Y. Hong, K. Yoshimura, D. R. Cayan, and V. Misra (2013), A high-resolution ocean-atmosphere coupled downscaling of the present climate over California, *Clim. Dyn.*, doi:10.1007/s00382-013-1670-7, in press.
Li, H., M. Kanamitsu, S. -Y. Hong, K. Yoshimura, D. R. Cayan, V. Misra, and L. Sun (2014), Projected climate change scenario over California by a regional ocean-atmosphere coupled model system, *Clim. Change*, *122*(4), 609–619, doi:10.1007/s10584-013-1025-8.
Liu, H., C. Wang, S.-K. Lee, and D. B. Enfield (2012), Atlantic warm pool variability in the IPCC AR4 CGCM simulations, *J. Clim.*, *25*, 5612–5628.
Liu, H., C. Wang, S.-K. Lee, and D. B. Enfield (2015), Atlantic warm pool variability in the CMIP5 simulations, *J. Clim.*, *26*, 5315–5336.
Liu, Y., S.-K. Lee, B. A. Muhling, J. T. Lamkin, and D. B. Enfield (2012), Significant reduction of the loop current in the 21st century and its impact on the Gulf of Mexico, *J. Geophys. Res.*, *117*, C05039, doi:10.1029/2011JC007555.
Liu, Y., S.-K. Lee, D. B. Enfield, B. A. Muhling, J. T. Lamkin, F. Muller-Karger, and M. A. Roffer (2015), Potential impact of climate change on the Intra-Americas Seas: Part 1—A dynamic downscaling of the CMIP5 model projections, *J. Mar. Syst.*, *148*, 56–69, doi:10.1016/j.marsys.2015.01.007.
Maxwell, J. T., P. T. Soulé, J. T. Ortegren, and P. A. Knapp (2012), Drought-busting tropical cyclones in the Southeastern Atlantic United States: 1950–2008, *Ann. Assoc. Am. Geogr.*, *102*(2), 259–275.
Maxwell, J. T., J. T. Ortegren, P. A. Knapp, and P. T. Soulé (2013), Tropical cyclones and drought amelioration in the gulf and Southeastern coastal United States, *J. Clim.*, *26*, 8440–8452.
McBride, J. L., and K. Fraedrich (1995), CISK: A theory for the response of tropical convective complexes to variations in sea surface temperature, *Q. J. R. Meteorol. Soc.*, *121*, 783–796, doi:10.1002/qj.49712152404.
Mellor, G. L., and T. Yamada (1982), Development of a turbulence closure model for geophysical fluid problems, *Rev. Geophys.*, *20*, 851–875, doi:10.1029/RG020i004p00851.
Mellor, G. L., T. Ezer, and L.-Y. Oey (1994), The pressure gradient conundrum of sigma coordinate ocean models, *J. Atmos. Ocean Modell.*, *13*, 166–175.
Misra, V. (2013), A multi–disciplinary assessment of the southeastern United States Climate, *Reg. Environ. Change*, *13*, S1–3.
Misra, V., and S. Bastola (2015), Reconciling droughts and landfalling tropical cyclones in the Southeastern United States, *Clim. Dyn.*, doi:10.1007/s00382-015-2645-7, in press.
Misra, V., and S. DiNapoli (2013), Understanding wet season variations over Florida, *Clim. Dyn.*, *40*, 1361–1372.
Misra, V., S. Chan, R. Wu, and E. Chassignet (2009), Air-sea interaction over the Atlantic warm pool in the NCEP CFS, *Geophys. Res. Lett.*, *36*, L15702, doi:10.1029/2009GL038737.
Misra, V., et al. (2011a), Climate Scenarios: A Florida-centric view: A white paper on climate scenarios for Florida. [Available at http://floridaclimate.org/docs/climate_scenario.pdf.]
Misra, V., L. Moeller, L. Stefanova, S. Chan, J. J. O'Brien, T. J. SmithIII, and N. Plant (2011b), The influence of Atlantic warm pool on Panhandle Florida sea breeze, *J. Geophys. Res.*, *116*, D00Q06, doi:10.1029/2010JD015367.
Mooers, C. (1998), Intra-Americas circulation, in *The Sea, the Global Coastal Ocean, Regional Studies and Syntheses*, pp. 183–208, John Wiley.
Moorthi, S., and M. J. Suarez (1992), Relaxed Arakawa-Schubert: A parameterization of moist convection for general circulation models, *Mon. Weather Rev.*, *120*, 978–1002, doi:10.1175/1520-0493(1992)120<0978:RASAPO>2.0.CO;2.
Neelin, J., C. Chou, and H. Su (2003), Tropical drought regions in global warming and El Nino teleconnections, *Geophys. Res. Lett.*, *30*(24), 2275, doi:10.1029/2003GL018625.
Ortegren, J. T., and J. T. Maxwell (2014), Spatiotemporal patterns of drought/tropical cyclone co-occurrence in the Southeastern USA: Linkages to north Atlantic climate variability, *Geogr. Compass*, *8*, 540–559, doi:10.1111/gec3.12148.
Pielke, R. A. (1974), A three-dimensional numerical model of the sea breezes over south Florida, *Mon. Weather Rev.*, *102*(2), 115–139.
Pielke, R. A., Jr., J. Gratz, C. W. Landsea, D. Collins, M. A. Saunders, and R. Musulin (2008), Normalized hurricane damage in the United States: 1900–2005, *Nat. Hazards Rev.*, *9*, 29–42.
Rappaport, E. N., J. L. Franklin, A. B. Schumacher, M. DeMaria, L. K. Shay, and E. J. Gibney (2010), Tropical intensity change before U. S. Gulf coast landfall, *Weather Forecast.*, *25*, 1380–1396.
Rauscher, S., A. Kucharski, and D. Enfield (2011), The role of regional SST warming variations in the drying of Meso-America in future climate projections, *J. Clim.*, *24*, 2003–2016.
Reynolds, R. W., and D. B. Chelton (2010), Comparisons of daily sea surface temperature analyses for 2007–08, *J. Clim.*, 3545–3562.
Reynolds, R. W., T. M. Smith, C. Liu, D. B. Chelton, K. S. Casey, and M. G. Schlax (2007), Daily high-resolution-blended analyses for sea surface temperature, *J. Clim.*, *20*, 5473–5496, doi:10.1175/2007JCLI1824.1.
Rousset, C., and L. M. Beal (2010), Observations of the Florida and Yuctan Currents from a Caribbean Cruise Ship, *J. Phys. Oceanogr.*, *40*, 1575–1581.
Schlitz, R. J., (1973), Net total transport and net transport by water mass categories for Yucatan Channel, based on data for April 1970. Ph.D. dissertation, Texas A&M University, 107 pp.
Selman, C., and V. Misra (2015), Simulating diurnal variations over the southeastern United States, *J. Geophys. Res. Atmos.*, *120*, 180–198, doi:10.1002/2014JD021812.
Selman, C., V. Misra, L. Stefanova, S. DiNapoli, and T. J. Smith III (2013), On the twenty-first-century wet season projections over the Southeastern United States, *Reg. Environ. Change*, *13*, S153–S164, doi:10.1007/s10113-013-0477-8.
Shchepetkin, A. F., and J. C. McWilliams (2005), The regional oceanic modeling system (ROMS): A split-explicit, free-surface, topography-following-coordinate ocean model, *Ocean Modell.*, *9*, 347–404.

Sikiric, M. D., I. Janekovic, and M. Kuzmic (2009), A new approach to bathymetry smoothing in sigma-coordinate ocean models, *Ocean Modell.*, *29*, 128–136.

Stommel, H. (1948), The westward intensification of wind-driven ocean currents, *Trans. AGU*, *29*, 202–206, doi:10.1029/TR029i002p00202.

Tiedtke, M. (1983), The sensitivity of the time-mean large-scale flow to cumulus convection in the ECMWF model, in *Proceedings of ECMWF Workshop on Convective in Large-Scale Models*, pp. 297–316, Eur. Cent. for Medium-Range Weather Forecasts, Reading, U. K.

Umlauf, L., and H. Burchard (2003), A generic length-scale equation for geophysical turbulence models, *J. Mar. Res.*, *61*, 235–265, doi:10.1357/002224003322005087.

Wang, C., S. Dong, and E. Munoz (2010), Seawater density variations in the North Atlantic and the Atlantic meridional overturning circulation, *Clim. Dyn.*, *34*, 953–968, doi:10.1007/s00382-009-0560-5.

Xie, P., A. Yatagai, M. Chen, T. Hayasaka, Y. Fukushima, C. Liu, and S. Yang (2007), A gauge based analysis of daily precipitation over East Asia, *J. Hydrometeorol.*, *8*, 607–626.

Xie, S., C. Deser, G. Vecchi, J. Ma, H. Teng, and A. Wittenberg (2010), Global warming pattern formation: Sea surface temperature and rainfall, *J. Clim.*, *23*, 966–986.

Zhang, L., C. Wang, and S.-K. Lee (2014), Potential role of Atlantic warm pool-induced freshwater forcing in the Atlantic meridional overturning circulation: Ocean-sea ice coupled model simulations, *Clim. Dyn.*, doi:10.1007/s00382-013-2034-z, in-press.